Oil & Gas Science and Technology – Rev. IFP Energies nouvelles (2017) **72**, 9

DOI: 10.2516/ogst/2017004

Experimental Optimization and Modeling of Sodium Sulfide Production from H_2S-Rich Off-Gas via Response Surface Methodology and Artificial Neural Network

Fatemeh Bashipour[1]*, Amir Rahimi[2], Saied Nouri Khorasani[3] and Abbas Naderinik[4]

[1] Faculty of Petroleum and Chemical Engineering, Razi University, Kermanshah 67149-67346 - Iran
[2] Department of Chemical Engineering, College of Engineering, University of Isfahan, Isfahan 81746-73441 - Iran
[3] Department of Chemical Engineering, Isfahan University of Technology, Isfahan 84156-83111 - Iran
[4] Iran Chemical Industrial Investment Company, Isfahan 81587-14311 - Iran
e-mail: f.bashipour@razi.ac.ir - rahimi@eng.ui.ac.ir - saied@cc.iut.ac.ir - ab.naderinik@gmail.com

* Corresponding author

Abstract *— The existence of hydrogen sulfide (H_2S) in the gas effluents of oil, gas and petrochemical industries causes environmental pollution and equipment corrosion. These gas streams, called off-gas, have high H_2S concentration, which can be used to produce sodium sulfide (Na_2S) by H_2S reactive absorption. Na_2S has a wide variety of applications in chemical industries. In this study, the reactive absorption process was performed using a spray column. Response Surface Methodology (RSM) was applied to design and optimize experiments based on Central Composite Design (CCD). The individual and interactive effects of three independent operating conditions on the weight percent of the produced Na_2S (Y) were investigated by RSM: initial NaOH concentration (10-20% w/w), scrubbing solution temperature (40-60 °C) and liquid-to-gas volumetric ratio (15×10^{-3} to 25×10^{-3}). Furthermore, an Artificial Neural Network (ANN) model was used to predict Y. The results from RSM and ANN models were compared with experimental data by the regression analysis method. The optimum operating conditions specified by RSM resulted in Y of 15.5% at initial NaOH concentration of 19.3% w/w, scrubbing solution temperature of 40 °C and liquid-to-gas volumetric ratio of 24.6×10^{-3} v/v.*

Résumé — Optimisation expérimentale et modélisation de la production de sulfure de sodium à partir d'H_2S riche en gaz provenant de la surface d'intervention méthodologique et de réseau de neurones artificiels — La présence de sulfure d'hydrogène (H_2S) dans les effluents gazeux rejetés par l'industrie pétrolière, gazière et pétrochimique entraîne une pollution de l'environnement ainsi que la corrosion des équipements. Ces flux gazeux, appelés effluents gazeux, présentent une forte concentration de H_2S qui peut être employée pour produire du sulfure de sodium (Na_2S) par absorption réactive de H_2S. Le Na_2S trouve une multitude d'applications dans les industries chimiques. Dans cette étude, le processus d'absorption réactive a été réalisé avec une colonne à pulvérisation. La méthode des surfaces de réponses (*Response Surface Methodology*, RSM) a été appliquée pour concevoir et optimiser des expériences basées sur les plans composites centrés (*Central Composite Design*, CCD). Les effets individuels et interactifs de trois conditions d'exploitation indépendantes sur le pourcentage en poids de Na_2S produit (*Y*) ont été analysés par RSM, à savoir : la concentration de NaOH initiale (10 à 20 % p/p), la température de la solution de lavage (40 à 60 °C) et le rapport du volume liquide/gaz (15×10^{-3}-25×10^{-3}). Un modèle de

réseau de neurones artificiels (*Artificial Neural Network*, ANN) a en outre servi à prédire *Y*. Les résultats issus des modèles de RSM et d'ANN ont été comparés aux données expérimentales par analyse de régression. Les conditions d'exploitation optimales spécifiées par la RSM ont donné pour *Y* un résultat de 15,5 % à une concentration de NaOH initiale de 19,3 % p/p, à une température de solution de lavage de 40 °C et à un rapport du volume liquide/gaz de 24,6 × 10^{-3} v/v.

INTRODUCTION

Many effluent gas streams in oil, gas and petrochemical industries, called off-gas, are similar to gases resulting from thermal cracking and hydrotreating plants, which contain hydrogen sulfide (H_2S). The existence of H_2S in the off-gas can cause environmental pollution and equipment corrosion. H_2S is a highly toxic gas which has a narcotic effect on the nervous system including paralysis of the olfactory nerves. The sense of smell can no longer be relied upon after a short exposure [1]. Depending on H_2S concentration, composition and flow rate of the off-gas, and the desired specifications of the refined off-gas, there are many commercial processes for H_2S removal from the off-gas streams. The most common and widely used methods of removing H_2S are absorption into alkaline solution, physical absorption, oxidation, dry sorption, membrane permeation and adsorption [2, 3]. H_2S absorption into NaOH solution is one of the main methods to produce sodium sulfide (Na_2S) and H_2S removal. Other methods to produce Na_2S are reduction of sodium sulfate (Na_2SO_4) by solid carbonaceous materials, reduction of Na_2SO_4 by gaseous reducing agents, exchange decomposition of barium sulfide (BaS) with sodium sulfate, carbonate, and hydroxide as well as an electrolytic method [4]. When off-gas contains high concentrations of H_2S, producing Na_2S becomes feasible alongside H_2S removal from off-gas using absorption into NaOH solution. In other words, Na_2S production and H_2S removal from off-gas can occur simultaneously in one process. However, when the main objective of the process is H_2S removal from off-gas and considering the fact that NaOH solution cannot be easily regenerated, NaOH scrubbers are most often applied for removing small quantities of acid gases containing H_2S [5, 6].

The absorption of H_2S from off-gas into NaOH solution results in production of Na_2S through two reversible reactions:

$$H_2S_{(aq)} + NaOH_{(aq)} \leftrightarrow NaHS(aq) + H_2O_{(l)} \quad (1)$$

$$NaHS_{(aq)} + NaOH_{(aq)} \leftrightarrow Na_2S_{(aq)} + H_2O_{(l)} \quad (2)$$

Na_2S is highly hygroscopic, and its solubility in water increases with increasing temperature. This valuable product has a wide variety of applications in chemical industries: It is widely used in pulp and paper industries in the Kraft process, in leather and tanning industries as the depilation agent for raw hides, in textile industries as a bleach and mordant in dyeing cotton fabric, in the photography industry to protect developer solutions from oxidation, and in dyestuff and dye printing industries as a dye agent in solving thion dye and production of sulfur dyes. Na_2S is also used in pharmaceutical-grade chemicals production and in water treatment as an oxygen scavenger agent. It is also used as a metals precipitant in desulfurizing rayon and cellophane, elastomers, lubricants, and organic compounds, as well as in man-made fibers. Other applications include recovery of metals as the insoluble sulfides and ore flotation as a reducing agent, production of a sulfonation and sulfomethylation agent and sodium thiosulfate ($Na_2S_2O_3$) as well as sodium hydrosulfide (NaHS) in the medical and chemical industries [7-11].

The reactive absorption of H_2S from off-gas into NaOH solution to produce Na_2S can be performed in gas-liquid contactor devices such as spray, packed and tray columns. A spray column is an appropriate gas-liquid contactor device, because precipitation of Na_2S at normal temperatures may ordinarily clog the internal apparatus in a continuous process. In practice, a fine spray of NaOH solution is brought into contact with off-gas inside a spray column in order to remove H_2S by chemical absorption and produce Na_2S solution. High-efficiency, low-pressure drops, operability in a wide range of liquid-to-gas flow rate ratios and low investment costs are other advantages of using spray columns [12]. The high solubility of H_2S in NaOH solution and prevention of foaming are other reasons to use spray columns [12, 13].

There have been several studies on Na_2S and NaHS production by H_2S absorption into NaOH solution. Maschwitz studied a continuous process to produce a high-concentration NaHS solution in the range of 25-30% w/w by H_2S absorption from gas mixtures containing H_2S (0.25-20% w/w) and hydrocarbons into NaOH solution in packed columns [14]. Other works on production of NaHS solution utilized waste gas and waste soda liquid in oil refineries [15], and by reaction of Na_2S with pure H_2S in a closed-reaction system including a reaction chamber [16]. Akiba presented a production method of an anhydrous alkali metal sulfide such as anhydrous sodium sulfide by bubbling an alkali metal hydroxide solution in an aprotic organic solvent, with the hydrogen sulfide temperature between 50 and 250 °C [17].

Brons and Myers [18] studied a continuous process of putting heavy oils containing sulfuric compounds into contact with NaOH solution at a temperature of 380-450 °C for a sufficient time to form sodium sulfide (10% w/w) and removal of organically bound sulfur in the form of mercaptans, sulfides and thiophenes. Then, the produced Na_2S was used to form metal sulfides [18]. The results of our literature review indicate that there is no comprehensive information on production of Na_2S solution using high H_2S content (≈25% v/v) off-gas stream through reactive absorption process of H_2S into NaOH solution in a spray column.

In this study, Response Surface Methodology (RSM) was employed as a statistical method for design of experiments of reactive absorption of off-gas including H_2S into NaOH solution to produce Na_2S in a spray column. The experiments were performed at the *Iran Chemical Industrial Investment Company* (Isfahan, Iran) to use H_2S-rich off-gas from the effluent gas of the hydrotreating unit. RSM was applied to investigate the individual and interactive effects of initial NaOH concentration (C_0), scrubbing solution temperature (T) and liquid-to-gas volumetric ratio (L/G) on the weight percent of produced Na_2S (Y). The ranges of the above-mentioned parameters are 10-20% w/w, 40-60 °C, and 15×10^{-3} to 25×10^{-3} v/v, respectively. The range for C_0 was selected to maintain the scrubbing solution pH higher than 13.5, hence producing Na_2S to subsequently produce NaHS with higher selectivity, and to minimize sulfide precipitation problems [5, 19]. The range of 40-60 °C is suitable for T, because of the decrease in the rate of reactions (1) and (2) at lower temperatures and the decrease of the solubility of H_2S into NaOH solution at higher temperatures, thus decreasing Na_2S production [19]. For L/G, the satisfactory operation conditions were obtained in the range of 15×10^{-3} to 25×10^{-3} v/v. By applying L/G values outside of this range, operating problems such as coning and flooding phenomena take place. Within the mentioned ranges, RSM was used to optimize the operating conditions and determine the maximum value of Y.

In addition to applying the RSM model, the Artificial Neural Network (ANN) model was implemented to predict Y using MATLAB (Version 8.1.0.604). Furthermore, the model results were compared with experimental data by the coefficient of determination (R^2), Mean Square Error (MSE) and Absolute Average Deviation (AAD).

1 MATERIALS AND METHODS

1.1 Materials

H_2S-rich off-gas in the experiments was supplied from the effluent gas of the hydrotreating unit at the *Iran Chemical Industrial Investment Company* (Isfahan, Iran). The molar composition of the off-gas is 25.0% hydrogen sulfide, 33.1% hydrogen, 5.5% methane, 5.0% butane, 16.4% ethane, 11.7% propane, 0.6% iso-butane, 1.8% N-pentane, 0.4% iso-pentane and 0.5% C_{6+}. The NaOH solution of 10-20% w/w was prepared from the industrial grade of NaOH solution (47% w/w, *Bandar Imam petrochemical Co.*). All of the chemicals used for titration analyses of NaHS and Na_2S were obtained from *Merck Company* (95-99%).

1.2 Experimental Apparatus and Procedure

The experiments were carried out in a lab-scale spray column. Figure 1 shows the schematic diagram of the lab-scale plant for Na_2S production. The spray column was a stainless steel cylinder (5 cm ID × 103 cm) (5) including a shower head with several holes (2.3 mm ID). The flow rates of inlet and outlet gas streams to and from the spray column were measured by glass tube gas flow meters (AMC-RGD, *Azmoon motamam Co.*) (1, 9). Before off-gas loading the spray column, it was heated to the desired operating temperature of 40-60 °C by electric heaters (4). The H_2S content of off-gas in the inlet and outlet of the spray column were measured by Dräger-tubes (*Dräger Safety AG & Co. KGaA*) (2) which were suitable for H_2S detection in the range of 0.2-7% v/v and 2-40% v/v, respectively. In all experiments, inlet gas pressure and flow rate were set at 1 bar g and 100 L/min, respectively. The outlet gas stream from the spray column and H_2S analyzer section entered high-concentration NaOH solution tank (3). Subsequently, the outlet gas stream from the NaOH solution tank (3) was transferred to the furnace. Before releasing off-gas stream, the prepared NaOH solution in the range of 10-20% w/w were kept in the fresh NaOH solution tank (30 cm ID × 69 cm) (12). About 10 L of the solution were transferred to the collecting tank (46 cm ID × 37 cm) (6) for startup of experiments. The collecting tank was equipped with a mixer (7) and steam coils (8) to obtain a well-dispersed solution with the desired temperature.

The H_2S in the off-gas was absorbed into scrubbing NaOH solution in a counter-current pattern to produce Na_2S solution. Initially, before reaching steady state conditions for the scrubbing system, the NaOH solution in the collecting tank was recycled by the pump (10), and the valve belonging to the fresh NaOH solution tank (12) was kept closed. Samples were collected from the collection tank and their pH values were measured with a pH meter (*Metrohm Co.*) (18). When the sample pH was below 13.5, a fresh NaOH solution stream was added to the recycle stream by the pump (15) to keep pH $\geq$ 13.5 during absorption in order to produce Na_2S instead of NaHS. The fresh NaOH solution was heated to the desired operating temperature by electric heaters (14) before being fed into the

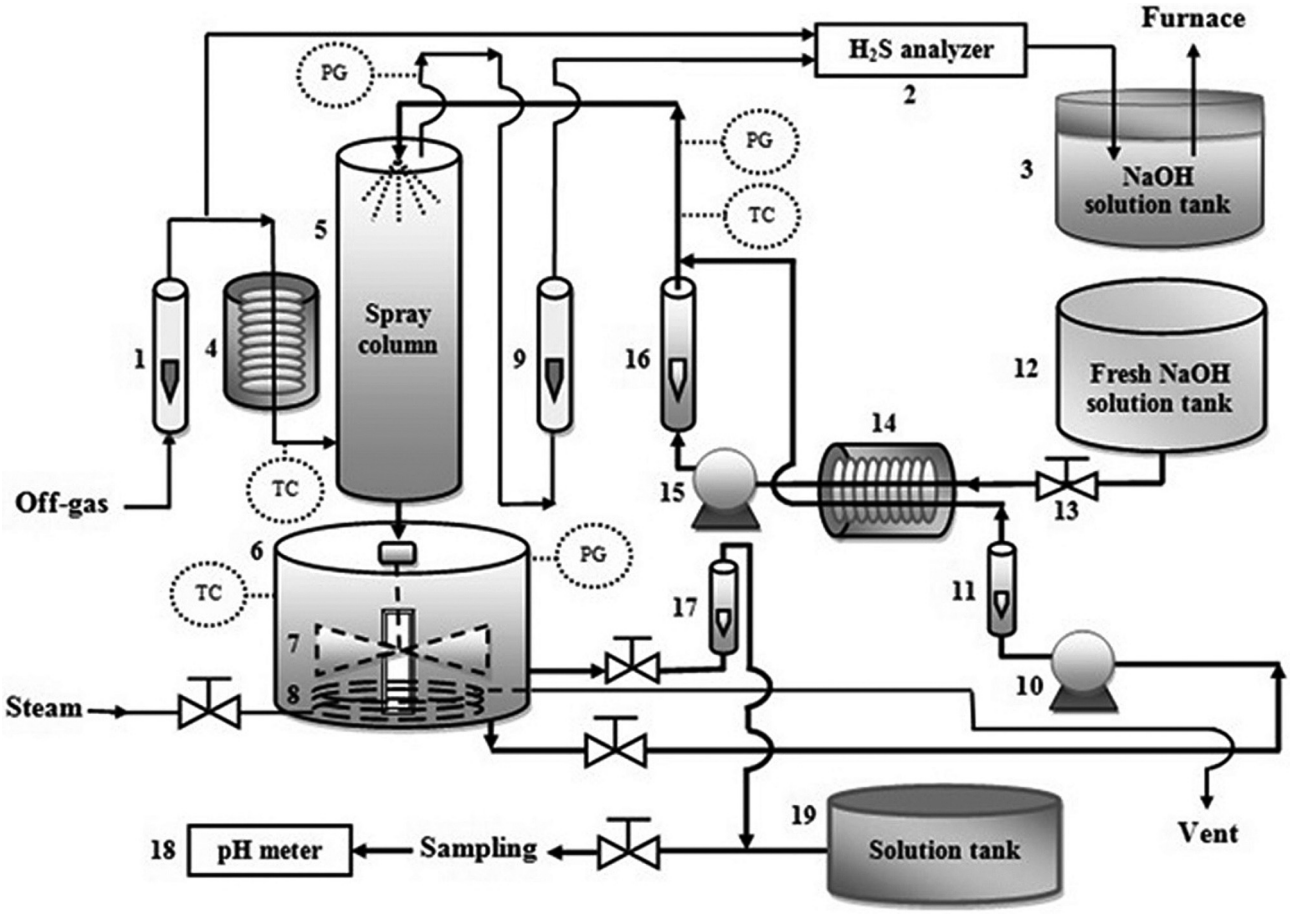

Figure 1

Schematic diagram of the lab-scale plant for Na_2S production: (1) and (9) gas flow meters, (2) H_2S analyzer, (3) NaOH solution tank, (4) and (14) electric heaters; (5) spray column, (6) collecting tank, (7) mixer, (8) steam coils, (10) and (15) pumps, (11), (16) and (17) rotameters, (12) fresh NaOH solution tank, (13) valve, (18) pH-meter, (19) solution tank and PG: Pressure Gauge, TC: Temperature Controller.

spray column. In steady state operation of the continuous process, the flow rate of fresh NaOH solution was equivalent to the liquid outlet stream from the spray column. The flow rates of liquid phases were controlled by the rotameters (11, 16, 17). The output solution stream was collected in the solution tank (19). When steady state was reached, the sampling was performed and kept for further titration analysis. The produced Na_2S solutions can reach commercial-grade quality by evaporating water from the solution. The water evaporation stage was not performed in this study.

1.3 Titration Analysis

All collected samples were analyzed by standard titration technique with aqueous hydrochloric acid (HCl) to determine concentration of sulfides [20]. The weight percent of each component of Na_2S, NaHS and NaOH in the collected samples can be determined by this titration analysis. Thymolphthalein and bromophenol were used as indicators to determine the content of Na_2S and NaHS in solution, respectively.

2. APPLIED MODELS AND EXPERIMENTAL DESIGN

2.1 RSM Model and Experimental Design

RSM is a mathematical and statistical technique that is based on fitting a full quadratic model to the experimental data [21, 22]. There are three stages in RSM: (1) design of experiments specified by response variables, independent variables and their levels and statistical procedure such as Central Composite Design (CCD); (2) carrying out the designed experiments and applying regression analysis using RSM to obtained results; (3) optimization of response surface model. Additionally, RSM allows evaluating the statistical significance of individual process variables, as well as the interaction between variables [23-25].

RSM was employed to investigate the effect of the variables of initial NaOH concentration (X_1), scrubbing solution temperature (X_2) and liquid-to-gas volumetric ratio (X_3) and their interactions on the weight percent of the produced Na_2S (Y). CCD with three variables (C_0, T and L/G) and three levels was used to obtain the optimum conditions for Na_2S production. RSM fitted a full-quadratic equation with the experimental data to provide a reasonable response surface modeling through regression analysis in MINITAB software (version 16). In order to investigate the effects of variables with different magnitude of value, coded variables (Z_i) were applied instead of uncoded variables (X_i, i = 1-3). These variables were coded by the following equation:

$$Z_i = \frac{X_i - X_{i.c}}{\Delta X_i} \tag{3}$$

where X_i, $X_{i.c}$ and ΔX_i are the real value, real value at center point and step change in the variable i (i = 1-3), respectively. Table 1 shows the coded and uncoded levels of independent variables employed in RSM design. The experiments randomly designed by RSM involved six axial points and eight cube points which repeated twice, and six center points.

As mentioned earlier, RSM provides a second-order - polynomial equation including linear and quadratic variables with interaction terms [26] as in Equation (4):

$$Y = \beta_0 + \sum_{i=1}^{3} \beta_i Z_i + \sum_{i=1}^{3} \beta_{ii} {Z_i}^2 + \sum_{i=1}^{2} \sum_{j=i+1}^{3} \beta_{ij} Z_i Z_j + \varepsilon \tag{4}$$

where Y represents the response variable (weight percent of produced Na_2S), Z_i is a coded variable, β_0, β_i, β_{ii}, β_{ij} are regression coefficients for the constant term, the square term and the interaction term, respectively, and ε is residual factor associated with the experiments.

The statistical analysis of the RSM was carried out in the form of analysis of variance (ANOVA) which presents the sources of variation, the degrees of freedom, sum of squares and the mean square for the model. ANOVA also includes F-value and probability (p-values) employed to determine whether the predictors or factors are significantly related to the response. In addition to ANOVA, R^2 and the adjusted coefficient of determination (Adj. R^2) were applied to verify the model validity.

TABLE 1
Coded and uncoded levels of independent variables employed in RSM design.

	Uncoded variables (X_i)		
	X_1	X_2	X_3
Coded variables (Z_i)	Initial NaOH concentration (C_0), [% w/w]	Scrubbing solution temperature (T), [°C]	Liquid-to-gas volumetric ratio (L/G) × 10^3, [v/v]
−1	10	40	15
0	15	50	20
1	20	60	25

2.2 ANN Model Description

ANN is an alternative modeling tool to the polynomial regression model, which can describe the complex nonlinear relationships between experimental data. A common ANN architecture is a Multi-Layer Feed Forward (MLFF) network. It consists of an input layer, one or more hidden layers and an output layer. Each layer involves processing units called neurons which operate independently of others [27, 28]. In the current study, a MLFF network was applied with the architecture as shown in Figure 2: an input layer included three operating conditions as input neurons, an output layer with one neuron, and one hidden layer which its neurons can change to gain the best ANN performance. The selection of one hidden layer was sufficient for accurate statistical prediction.

An ANN model inherently needs more experimental data than RSM to have an efficient and accurate prediction. But, ANN can also build a satisfactory model even with relatively less data, if the data were collected from experiments that matching the experimental design [29]. The relationship between the components of a MLFF network can be represented by the following equation:

$$y_{jk} = F_k\left(\sum_{i=1}^{N_{k-1}} w_{ijk} y_{i(k-1)} + b_{jk}\right) \tag{5}$$

where y_{jk} is the neuron j's output from k's layer, b_{jk} is the bias weight for neuron j in layer k, and w_{ijk} are the weights representing the strength of the connection between the ith neuron and jth neuron. F_k is the activation transfer functions. Three types of activation transfer functions were used: sigmoidal function, hyperbolic tangent and linear function. Sigmoidal function is the most common activation transfer function [30, 31].

The MLFF optimization was carried out in four stages: (1) determining the Back-Propagation Learning Algorithm (BPLA); (2) specifying the optimum number of neurons in the hidden layer; (3) estimating the initial values of

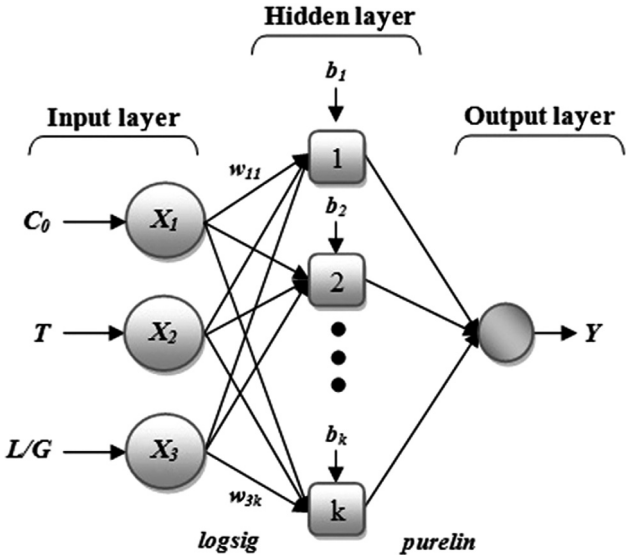

Figure 2

Architecture of the three-layered MLFF network.

weights and biases for Equation (5); (4) updating the weights and biases to obtain optimum ANN performance up to the minimum network error like MSE. Since the experimental data used in ANN had different ranges, all input and output experimental data were normalized to the range of 0-1. This data normalization was performed to prevent disorder in the learning process and gain homogenous results and higher ANN performance [32, 33].

3 RESULTS AND DISCUSSION

3.1 Analysis of RSM

In this study, a set of 20 experiments was employed to obtain the full quadratic model using CCD with three independent variables and three levels for each variable. This design of experiments was used to evaluate both the individual and the interactive effects of the operating conditions, and to determine the optimal operating conditions. Table 2 shows the set of 20 runs for experimental and predicted Y as the results of the experiments.

Table 3 shows the calculated coefficients of the regression model (Eq. 4). Statistical tests of t-value and p-value from Table 3 were employed to clarify the significance of each term in Equation (4). In this study, highly significant, significant and insignificant coefficients have p-value < 0.001, $0.001 \leq p$-value < 0.05 and p-value ≥ 0.05, respectively. Therefore, the quadratic polynomial model without insignificant coefficients for Y was obtained as the following equation:

$$Y = 12.5268 + 3.0104\,Z_1 - 0.3600\,Z_2 + 0.3994\,Z_3 - 1.6275{Z_1}^2 - 0.5467\,Z_1Z_2 - 0.4787\,Z_2Z_3 \pm 0.05 \quad (6)$$

The results presented in Table 3 indicate that linear and square C_0 were highly significant (p-value < 0.001). On the other hand, due to the effectiveness of C_0 on the prime cost and the possibility of creating the operating problems, its importance will be doubled. The linear terms of T and L/G, and all the interaction terms except C_0-L/G were significant ($0.001 \leq p$-value < 0.05). The other terms containing the square terms of T and L/G and the interaction term C_0-L/G were insignificant.

Analysis of variance for Y as a response surface quadratic model is presented in Table 4 and includes the statistic tests of F-value and p-values. In Table 4, p-value ≥ 0.05 for the lack-of-fit and p-value ≤ 0.001 for the regression model of Y obtained via analysis of variance (ANOVA) confirmed the fitted model. R^2 and Adj. R^2 employed to validate the RSM model were calculated to be 0.9824 and 0.9666, respectively. These values indicated that the model developed by RSM precisely agrees with the experimental results.

3.2 ANN Model

The weight percent of the produced Na_2S was modeled by MLFF network on the basis of operating conditions as input data. In this work, a three-layered network as shown in Figure 2 was used applying the log-sigmoid transfer function called "logsig" at the hidden layer and a linear transfer function called "purelin" at the output layer. Logsig and purelin transfer functions are defined by the following equations:

$$\text{logsig}(u) = \frac{1}{1 + e^{-u}} \quad (7)$$

$$\text{purelin}(u) = u \quad (8)$$

The optimum BPLA and number of neurons in the hidden layer were identified by trial-and-error. The best ANN performance was determined based on the minimum MSE of the training and prediction set. Seventy five percent of the CCD experimental data with two replications was randomly applied in the training process and the remaining 25% was used in test and validation processes. Table 5 shows the calculated MSE for different sets of ANN parameters. The results represented in Table 5 indicate that applying the logsig activation transfer function, Levenberg-Marquardt (L-M) learning algorithm, and five neurons in one hidden layer for the MLFF results in the minimum MSE. As shown

TABLE 2
Experimental and predicted data by RSM and ANN models for Y from the set of experiments performed based on CCD.

Run No.	X_1	X_2	$X_3 \times 10^3$	Y (% w/w)		
				Experimental ± 0.05	Predicted by RSM	Predicted by ANN
1	15	50	20	12.19	12.53	12.68
2	10	60	25	7.92	7.70	7.91
3	15	60	20	11.90	12.56	11.97
4	10	40	25	8.01	8.29	7.65
5	15	50	20	12.85	12.53	12.68
6	15	50	25	12.18	12.40	12.24
7	15	40	20	13.76	13.28	13.81
8	20	60	25	13.12	12.94	13.34
9	15	50	20	12.42	12.53	12.68
10	20	50	20	13.48	13.91	13.02
11	20	40	15	13.47	13.65	13.54
12	15	50	15	11.65	11.60	11.74
13	15	50	20	12.15	12.53	12.68
14	15	50	20	12.85	12.53	12.68
15	10	60	15	8.11	8.17	8.28
16	20	40	25	15.81	15.71	15.78
17	10	50	20	8.14	7.89	8.07
18	15	50	20	13.05	12.53	12.68
19	10	40	15	6.70	6.84	6.61
20	20	60	15	13.11	12.79	13.06

in Figure 3, this optimized MLFF network represents the best validation performance of MSE 2.4115×10^{-6}. Figure 4 shows the satisfactory agreement between the data predicted by ANN and experimental data.

3.3 Individual and Interactive Effects of Operating Conditions on *Y*

The operating conditions of C_0, T and L/G are three variables that affect spray column performance. Their individual and interactive effects on Y were investigated to find out the best experimental and efficient operating conditions. Three-dimensional response surfaces plots and two-dimensional contour plots can indicate the interactive effects of the independent variables on the response variable. These plots were visualized by the weight percent of the produced Na_2S *versus* initial NaOH concentration, scrubbing solution temperature and liquid-to-gas volumetric ratio in Figures 5 and 6. The third independent variable was kept at central point ($Z_i = 0$) in Figures 5 and 6.

Figure 5 shows the response surface and contour plots for the effect of initial NaOH concentration and liquid-to-gas volumetric ratio on Y at scrubbing solution temperature of 50 °C. Because of the direct effect of initial NaOH concentration on the production of Na_2S as described in Equations (1) and (2), C_0 is an important and efficient independent variable to increase Y. The main reason for the positive effects on Y of increasing C_0 is the enhancement of active and available moles of the absorbent solution which penetrates into gas-liquid interface and reacts with H_2S, thereby increasing the absorption rate and enhancement

TABLE 3
Calculated regression coefficients for quadratic polynomial model of *Y*.

Term	Coefficient	SE[a] coefficient	*t*-value	*p*-value
Constant	12.5268	0.1550	80.821	0.000
Z_1	3.0104	0.1426	21.115	0.000
Z_2	−0.3600	0.1426	−2.525	0.030
Z_3	0.3994	0.1426	2.801	0.019
Z_1^2	−1.6275	0.2719	−5.986	0.000
Z_2^2	0.3895	0.2719	1.432	0.183
Z_3^2	−0.5295	0.2719	−1.948	0.080
Z_1Z_2	−0.5467	0.1594	−3.430	0.006
Z_1Z_3	0.1520	0.1594	0.954	0.363
Z_2Z_3	−0.4787	0.1594	−3.003	0.013

[a] Standard Error.

TABLE 4
Analysis of variance (ANOVA) of the fitted quadratic polynomial model for *Y*.

Source	DF[a]	Seq. SS[b]	Adj. SS[c]	Adj. MS[d]	*F*-value	*p*-value[e]
Regression	9	113.462	113.462	12.6069	62.02	0.000
Linear	3	93.516	93.516	31.1721	247.07	0.000
Square	3	15.536	15.536	5.1785	25.48	0.000
Interaction	3	4.410	4.410	1.4700	7.23	0.007
Residual error	10	2.033	2.033	2.033		
Lack of fit	5	1.304	1.304	0.2607	1.79	0.270
Pure error	5	0.729	0.729	0.1458		
Total	19	115.495				

[a] Degree of freedom;
[b] Sequential sums of squares;
[c] Adjusted sum of squares;
[d] Adjusted mean squares;
[e] p-value < 0.001 highly significant; 0.001 ≤ p-value < 0.05 significant; p-value ≥ 0.05 not significant.

factor. Figure 5 confirms this activity within the range of the scrubbing solution temperatures. Moreover, Table 3 displays a positive linear effect of C_0 (p-value < 0.001) on the response variable. The increase in C_0 also had a negative effect on Y by increasing the density and viscosity of scrubbing solution. Therefore, H_2S molecular diffusion coefficients and H_2S solubility decrease due to acid-base equilibrium (Eq. 1 and 2), which reduces Y. Additionally, at constant pressure of the spray nozzle, the increase in density and viscosity of scrubbing solution led to production of drops with larger diameters, thus providing smaller liquid-gas interfaces. The positive and negative effects of initial NaOH concentration cancel each other and thus Y is almost independent of C_0 at $C_0 > 17.5\%$ w/w, especially at L/G higher than 20×10^{-3}, as shown in Figure 5. This effect is due to reciprocal positive linear (p-value < 0.001) and negative quadratic effects (p-value < 0.001) of Z_1 and negative Z_1-Z_2 interaction effect (p-value < 0.05) on

TABLE 5
Performance comparison of 15 ANN with different BLPA and number of neurons in the hidden layer.

BPLA	Function	N[a]	Epochs	MSE[b]	(R^2)[c]
BFGS quasi-Newton back-propagation	Trainbfg	5	9	4.4748×10^{-5}	0.8704
Conjugate gradient back-propagation with Powell-Beale restarts	Traincgb	5	31	7.6523×10^{-6}	0.9934
Conjugate gradient back-propagation with Fletcher-Reeves updates	Traincgf	5	32	3.5988×10^{-5}	0.9823
Conjugate gradient back-propagation with Polak-Ribiére updates	Traincgp	5	17	1.1361×10^{-4}	0.9327
Gradient descent with adaptive learning rate back-propagation	Traingda	5	240	7.4223×10^{-5}	0.9233
Gradient descent with momentum back-propagation	Traingdm	5	1000	1.2444×10^{-4}	0.4658
Gradient descent with momentum and adaptive learning rate back-propagation	Traingdx	5	261	7.8924×10^{-5}	0.9414
Levenberg-Marquardt back-propagation	Trainlm	5	10	2.4115×10^{-6}	0.9953
One-step secant back-propagation	Trainoss	5	9	1.0892×10^{-4}	0.8508
Resilient back-propagation	Trainrp	5	40	2.1994×10^{-5}	0.9922
Scaled conjugate gradient back-propagation	Trainscg	5	15	4.9185×10^{-5}	0.9517
Levenberg-Marquardt back-propagation	Trainlm	2	24	9.6908×10^{-5}	0.9833
Levenberg-Marquardt back-propagation	Trainlm	3	17	9.6355×10^{-6}	0.9936
Levenberg-Marquardt back-propagation	Trainlm	4	16	9.6565×10^{-6}	0.9919
Levenberg-Marquardt back-propagation	Trainlm	6	11	1.0432×10^{-5}	0.9923

[a] N is number of neurons in the hidden layer;
[b] MSE values are the best validation performance of the used ANN;
[c] R^2 values are related to all data involved the training, validation and test data set.

Álvarez-Cruz *et al.* obtained similar results regarding the effect of C_0 on H_2S absorption [5]. They concluded at higher concentration of NaOH solution (1 and 2 M), H_2S dissolution was less. In addition, Yincheng *et al.* studied the effect of initial NaOH and NH_3 concentration on CO_2 removal efficiency and acquired similar results with this study [34].

Increase in scrubbing solution temperature had two effects on *Y*. Increasing the scrubbing solution temperature

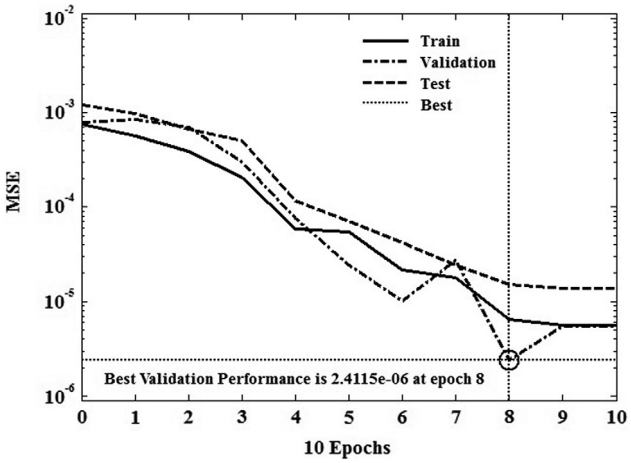

Figure 3

Plot of MSE of predicted data by ANN model and experimental results *versus* epochs.

provided positive effects on Y by increasing the rate of reactions (1) and (2) to produce more Na_2S, reducing the solution viscosity and, therefore, producing drops with smaller diameter and more liquid-gas interfacial area. In addition, increasing the scrubbing solution temperature leads to negative effects on Y due to:

1. decrease in H_2S solubility in scrubbing solution;
2. release of H_2S from solution to gas phases due to exothermic reactions of (1) and (2);
3. increase in water evaporation rate from solution, and therefore, increase in resistance against H_2S transition to liquid phase.

As summarized in Table 3, the scrubbing solution temperature had a negative linear (p-value < 0.05) effect and the negative interaction of Z_1-Z_2 (p-value < 0.05) and Z_2-Z_3 (p-value < 0.05) effects on Y. The effect on Y scrubbing solution temperature varied depending on which effect was dominant. The reciprocal effects of L/G and T at C_0 15% w/w in the surface and contour plots of Figure 6 show that the negative effects of T on Y were generally dominant in the considered range for T.

The prediction of spray column performance is difficult due to the complexity of its hydrodynamics. The spray column performance is influenced by several droplet specifications: size, distribution, velocity, collision, distortion, internal recirculation, and oscillation and coalescence between droplets [35]. Additionally, L/G is an effective and important design parameter for absorption columns from a process economics perspective. Increasing L/G can occur by increase in liquid flow rate or decrease in gas flow rate. Increasing liquid flow rate at constant gas flow rate resulted in L/G enhancement, the diameter of droplets increased at constant spraying pressure and therefore, the total liquid-gas interfacial area and hence Y were increased. This enhancement of Y occurs due to some reasons: (1) the reactive absorption of H_2S at the liquid film of NaOH solution (Hatta number > 2) [36]; (2) increasing collision of droplet and gas; (3) increase in mass transfer coefficient of gas because of increased velocity of droplets. Increasing L/G could cause a negative effect on Y by increasing both the rate of droplet coalescence and the thickness of liquid film on the wall of the spray column, thereby reducing liquid-gas interfacial area. On the other hand, the droplet coalescence raises the weight of droplets and the droplet falling rate which in turn reduces the contact time of two phases and therefore a decrease in Y. Figure 5 shows that Y increased approximately 11% by enhancement of L/G from 15×10^{-3} to 21.5×10^{-3} (v/v) and then remained constant, because the positive and negative effects of L/G enhancement cancel each other. Bandyopadhyay and Biswas obtained similar results in spray columns for the effect of L/G on SO_2 scrubbing using water and dilute NaOH [37] and for CO_2 capture into NaOH solution [38]. Their experimental results of reference [37] in a range of L similar to this study support the claim that increasing L/G from 15×10^{-3} to 18.6×10^{-3} at constant G of 6 Nm^3/h, increases the sauter mean diameter (d_{32}) of drops 17.6% and 5.6% of the total droplet surface area, although it decreases the number of droplets 23.6%. Zhang *et al.* acquired the same trend for the effect of L/G on the removal efficiency of SO_2 using seawater as an absorbent [39]. Both Figure 5 and the interaction coefficient of Z_1-Z_3 with p-value ≥ 0.05 in Table 3 show that the interaction effect of Z_1-Z_3 on Y was negligible.

As mentioned earlier, T and L/G had two effects on Y. Figure 6 indicates that the interaction of T and L/G with the coefficient of -0.4787 and p-value < 0.05 presented in Table 3 had a significant effect on Y.

3.4 Comparison Between Results of RSM and ANN Models

The precision and accuracy of RSM and ANN models were compared using R^2, MSE and AAD values. Table 6 shows that the ANN model with larger R^2 and smaller MSE and AAD values is superior to the RSM model in predicting Y. Additionally, the ANN model is not limited to number of experiments and it is applicable to complicated non-linear processes [21, 28].

3.5 Optimization of Operating Conditions

The optimum Y is predicted by analytical optimization of RSM. RSM estimated the sets of operating conditions that resulted in maximum Y (15.7 ± 0.1% w/w). These sets of operating condition were employed to determine the

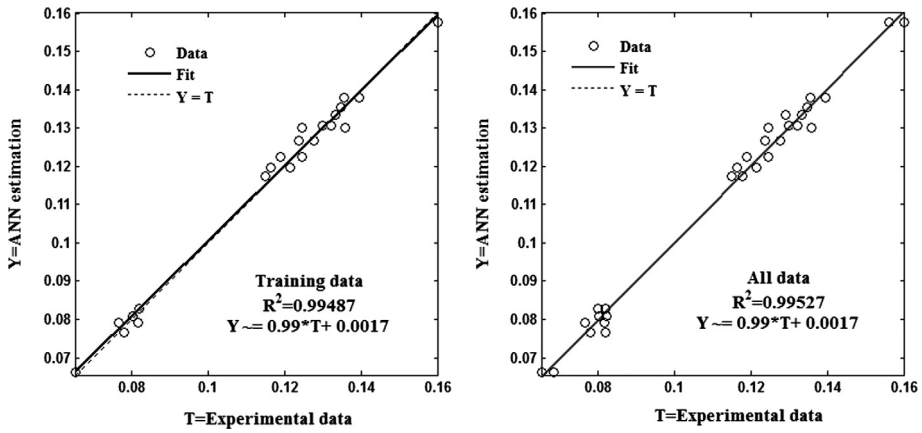

Figure 4

Scattergram of modeled normalized *Y* by ANN *versus* exprimental normalized *Y* for training and all data.

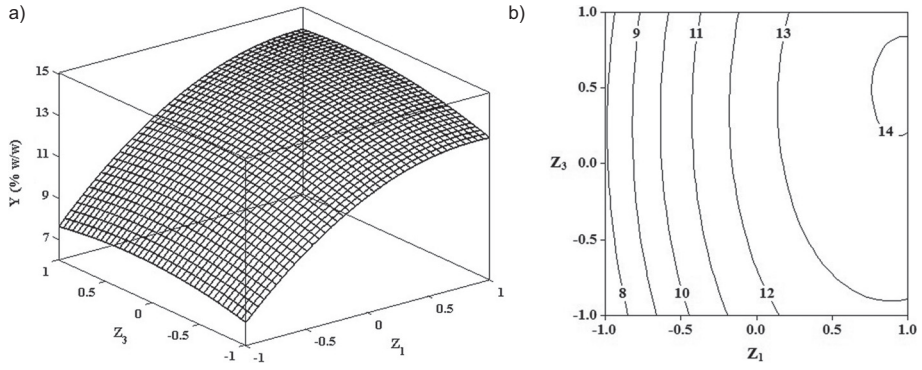

Figure 5

Response surface a) and contour b) plots for the effect of initial NaOH concentration and liquid-to-gas volumetric ratio on Y at scrubbing solution temperature of 50 °C.

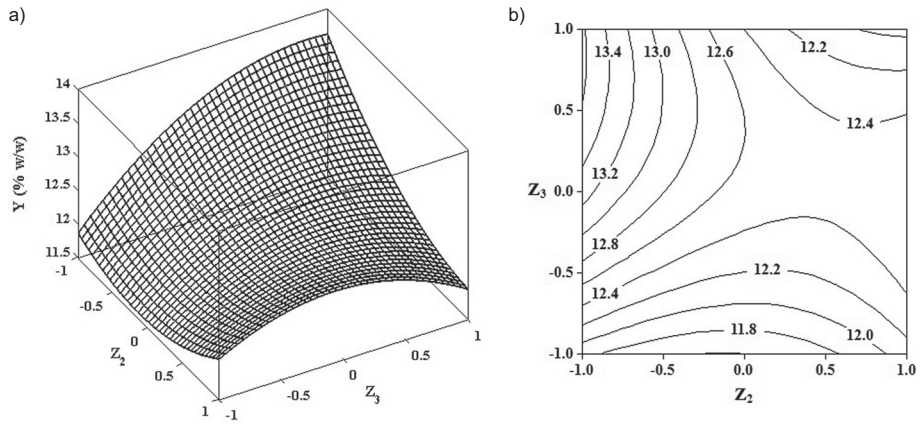

Figure 6

Response surface a) and contour b) plots for the effect of scrubbing solution temperature and liquid-to-gas volumetric ratio on *Y* at initial NaOH concentration of 20% w/w.

TABLE 6
Comparison of precision and accuracy of RSM and ANN models.

Model	$R^2 = 1 - \sum_{i=1}^{n} \left(Y_i - \hat{Y}_i\right)^2 / \sum_{i=1}^{n} \left(Y_i - \bar{Y}_i\right)^2$	$\text{MSE} = \frac{1}{n} \sum_{i=1}^{n} \left(Y_i - \hat{Y}_i\right)^2$	$\%\text{AAD} = \frac{1}{n} \left(\sum_{i=1}^{n} \left\lvert Y_i - \hat{Y}_i \right\rvert / Y_i \right) \times 100$
RSM	0.9824	0.1019	2.41
ANN	0.9953	2.4115×10^{-6}	1.66

* Y_i, $\hat{Y}_i$, and $\bar{Y}_i$ are the experimental data, modeling data and average of experimental data, respectively. n for RSM model is the number of experimental data and for ANN model is $n_{op} \times n_{dp}$ which n_{op} is the number of output parameters, and n_{dp} is the number of data patterns.

optimum operating conditions for maximum *Y*. The highest value of *Y* was predicted at initial NaOH concentration of 19.3% w/w, scrubbing solution temperature of 40 °C and liquid-to-gas volumetric ratio of 24.6×10^{-3}. The accuracy and precision of the *Y* model was validated with triplicate experiments giving an average *Y* of 15.5 ± 0.2% w/w.

CONCLUSION

The H_2S reactive absorption in the spray column into NaOH solution was employed to define the weight percent of the produced Na_2S insight from experimental, RSM and ANN models. The results show that Na_2S production from H_2S-rich off-gas is a suitable and reasonable way to achieve Na_2S besides removing the principal portion of H_2S from off-gas. Therefore, it can be applied as a pretreatment process. The effects of initial NaOH concentration, scrubbing solution temperature and liquid-to-gas volumetric ratio on *Y* were investigated. The experimental results showed that the linear and quadratic terms of initial NaOH concentration play a significant role on *Y*. Additionally, the linearity of scrubbing solution temperature and liquid-to-gas volumetric ratio and the interactions between initial NaOH concentration and scrubbing solution temperature, scrubbing solution temperature and liquid-to-gas volumetric had significant effects on the produced Na_2S.

An ANN model was developed, for which the results agreed well with experimental data when the MLFF network with the logsig activation transfer function, L-M training algorithm and 5 neurons in the single hidden layer was utilized. The comparison between the results of RSM and ANN models indicates that ANN model has higher precision than RSM model, based on comparison with the experimental data. However, both models could accurately describe *Y* based on regression analyses of R^2, MSE and AAD.

The maximum weight percent of the produced Na_2S of 15.5% was achieved at optimum operational conditions by a numerical and graphical analysis at an initial NaOH concentration of 19.3% w/w, scrubbing solution temperature of 40 °C and liquid-to-gas volumetric ratio of 24.6×10^{-3} v/v. The achieved Na_2S solution will be able to convert to the commercial-grade quality of Na_2S solution by evaporating excess water from the solution.

ACKNOWLEDGMENTS

The financial support for this study by *Iran Chemical Industrial Investment Company* (Isfahan, Iran) is gratefully acknowledged.

REFERENCES

1 Bahadori A. (2014) *Pollution Control in Oil, Gas and Chemical Plants*, Springer Cham Heidelberg, New York, Dordrecht, London.

2 Eimer D.A. (2014) *Gas treating absorption theory and practice*, John Wiley & Sons Ltd., Chichester, UK.

3 Kohl A.L., Nielsen R. (1997) *Gas Purification*, 5th edn., Gulf Professional Publishing, Houston, Texas.

4 Info Mine research group (2012) *Sodium sulfide and hydrosulfide production market and forecast in the CIS*, 2nd ed., Info Mine research group, Moscow.

5 Álvarez-Cruz R., Sánchez-Flores B.E., Torres-González J., Antaño-López R., Castañeda F. (2012) Insights in the development of a new method to treat H_2S and CO_2 from sour gas by alkali, *Fuel* **100**, 173-176.

6 Bashipour F., Nouri Khorasani S., Rahimi A. (2014) Mathematical modeling and genetic algorithm optimization of reactive absorption of hydrogen sulfide, *Chem. Eng. Technol.* **37**, 2175-2184.

7 Agarwal J. (2012) Effect of absorbability of iron contents by precipitated barium sulphate in the commercial crude sodium sulphide, *The IJST* **2**, 730-732.

8 Astarita G., Gioia F. (1964) Hydrogen sulphide chemical absorption, *Chem. Eng. Sci.* **19**, 963-971.

9 Lacasse K., Baumann W. (2004) *Textile chemicals: Environmental data and facts*, Springer-Verlag, Germany, pp. 557-558.

10 Peters R.W., Ku Y., Bhattacharyya D. (1985) Evaluation of recent treatment techniques for removal of heavy metals from industrial wastewaters, *AICHE J. Symposium Series* **81**, 165-203.

11 Speight J.G. (2002) *Chemical and process design handbook*, McGraw-Hill Inc., New York.

12 Turpin A., Couvert A., Laplanche A., Paillier A. (2008) Experimental study of mass transfer and H_2S removal efficiency in a spray tower, *Chem. Eng. Process.* **47**, 886-892.

13 Xia J., Pérez-Salado Kamps A., Rumpf B., Maurer G. (2000) Solubility of hydrogen sulfide in aqueous solutions of single strong electrolytes sodium nitrate, ammonium nitrate, and sodium hydroxide at temperatures from 313 to 393 K and total pressures up to 10 MPa, *Fluid Phase Equilibr.* **167**, 263-284.

14 Maschwitz P.A. (1953) *Process for manufacturing sodium hydrosulfide solution*, US Patent No. 2662000 A.

15 Yasuo U., Katsuo W. (1966) *Utilization of waste gas and waste soda liquid in oil refinery*, US Patent No. 3262753 A.

16 Manganaro J.L. (1984) *Production of sodium hydrosulfide*, US Patent No. 4439411 A.

17 Akiba L. (2002) *Method for the production of anhydrous alkali metal sulfide and alkali metal sulfide solution*, US Patent No. 6337062 B1.

18 Brons G., Myers R.D. (1997) *Contacting with sodium hydroxide to form sodium sulfide, contacting sodium sulfide with water and a transition metal to form transition metal sulfide, sodium hydroxide, hydrogen and impurities*, US Patent No. 5635056 A.

19 Mamrosh D., Beitler C., Fisher K., Stem S. (2008) Consider improved scrubbing designs for acid gases, *Hydrocarb. Process*, 1, 69-74.

20 Biermann C.J. (1996) *Handbook of pulping and papermaking*, 2nd edn., Academic Press, New York.

21 Bezerra M.A., Santelli R.E., Oliveira E.P., Villar L.S., Escaleira L.A. (2008) Response surface methodology (RSM) as a tool for optimization in analytical chemistry, *Talanta* **76**, 965-977.

22 Box G.E.P., Wilson K.B. (1951) On the experimental attainment of optimum conditions, *J. Roy. Stat. Soc. B Met.* **13**, 1-45.

23 Bashipour F., Ghoreishi S.M. (2014) Response surface optimization of supercritical CO_2 extraction of α-tocopherol from gel and skin of *Aloe vera* and almond leaves, *J. Supercrit. Fluids* **95**, 348-354.

24 Khan A.H., Shang J.Q., Alam R. (2014) Optimization of sample preparation method of total sulphur measurement in mine tailings, *Int. J. Environ. Sci. Technol.* **11**, 1989-1998.

25 Khosravi M., Rostami B., Fatemi S. (2012) Uncertainty Analysis of a Fractured Reservoir's Performance: A Case Study, *Oil Gas Sci. Technol.* **67**, 423-433.

26 Myers R.H., Montgomery D.C., Anderson-Cook C.M. (2009) *Response surface methodology: process and product optimization using designed experiments*, John Wiley & Sons, Inc., Hoboken, New Jersey.

27 Maran P.J., Sivakumar V., Thirugnanasambandham K., Sridhar R. (2013) Artificial neural network and response surface methodology modeling in mass transfer parameters predictions during osmotic dehydration of *Carica papaya L.*, *Alexandria Eng. J.* **52**, 507-516.

28 Bashipour F., Nouri Khorasani S., Rahimi A. (2015) H_2S reactive absorption from off-gas in a spray column: insights from experiments and modeling, *Chem. Eng. Technol.* **38**, 2137-2145.

29 Desai K.M., Survase S.A., Saudagar P.S., Lele S., Singhal R.S. (2008) Comparison of artificial neural network (ANN) and response surface methodology (RSM) in fermentation media optimization: case study of fermentative production of scleroglucan, *Biochem. Eng. J.* **41**, 266-273.

30 Jorjani E., Chehreh C.S., Mesroghli S.H. (2008) Application of artificial neural networks to predict chemical desulfurization of Tabas coal, *Fuel* **87**, 2727-2734.

31 Fausett L.V. (1993) *Fundamentals of neural networks: architectures, algorithms and applications*, Prentice-Hall, Englewood Cliffs, NJ.

32 Khajeh M., Moghaddam M.G., Shakeri M. (2012) Application of artificial neural network in predicting the extraction yield of essential oils of Diplotaenia cachrydifolia by supercritical fluid extraction, *J. Supercrit. Fluids* **69**, 91-96.

33 Chapoy A., Mohammadi A.H., Richon D. (2007) Predicting the hydrate stability zones of natural gases using artificial neural networks, *Oil Gas Sci. Technol.* **62**, 701-706.

34 Yincheng G., Zhenqi N., Wenyi L. (2011) Comparison of removal efficiencies of carbon dioxide between aqueous ammonia and NaOH solution in a fine spray column, *Energy Procedia* **4**, 512-518.

35 Codolo M.C., Bizzo W.A. (2013) Experimental study of the SO_2 removal efficiency and volumetric mass transfer coefficients in a pilot-scale multi-nozzle spray tower, *Int. J. Heat Mass Transfer* **66**, 80-89.

36 Gioia F., Astarita G. (1967) General solution to the problem of hydrogen sulfide absorption in alkaline solutions, *Ind. Eng. Chem. Fundam.* **6**, 370-375.

37 Bandyopadhyay A., Biswas M.N. (2008) Critical flow atomizer in SO_2 spray scrubbing, *Chem. Eng. J.* **139**, 29-41.

38 Bandyopadhyay A., Biswas M.N. (2012) CO_2 capture in a spray column using a critical flow atomizer, *Sep. Purif. Technol.* **94**, 104-114.

39 Zhang D.N., Chen Q.Z., Zhao Y.X., Maeda Y., Tsujino Y. (2001) Stack gas desulfurization by seawater in Shanghai, *Water, Air, Soil Poll.* **130**, 271-276.

Manuscript submitted in June 2016
Manuscript accepted in January 2017
Published online in March 2017

Cite this article as: F. Bashipour, A. Rahimi, S. Nouri Khorasani and A. Naderinik (2017). Experimental Optimization and Modeling of Sodium Sulfide Production from H_2S-Rich Off-Gas via Response Surface Methodology and Artificial Neural Network, *Oil Gas Sci. Technol* **72**, 9.